Phase coexistence of complex fluids in shear flow

Peter D. Olmsted[a] and C-Y. David Lu[b]

[a] *Department of Physics, University of Leeds, Leeds, UK LS2 9JT. E-mail:*
p.d.olmsted@leeds.ac.uk
[b] *Departments of Physics and Chemistry & Center of Complex Systems, National Central*
University, Chung-li, 320 Taiwan. E-mail: dlu@joule.phy.ncu.edu.tw

We present some results of recent calculations of rigid rod-like particles in shear flow, based on the Doi model. This is an ideal model system for exhibiting the generic behavior of shear-thinning fluids (polymer solutions, wormlike micelles, surfactant solutions, liquid crystals) in shear flow. We present calculations of phase coexistence under shear among weakly-aligned (paranematic) and strongly-aligned phases, including alignment in the shear plane and in the vorticity direction (log-rolling). Phase coexistence is possible, in principle, under conditions of both common shear stress and common strain rate, corresponding to different orientations of the interface between phases. We discuss arguments for resolving this degeneracy. Calculation of phase coexistence relies on the presence of inhomogeneous terms in the dynamical equations of motion, which select the appropriate pair of coexisting states. We cast this condition in terms of an equivalent dynamical system, and explore some aspects of how this differs from equilibrium phase coexistence.

1 Introduction

Shear flow induces phase transitions and dynamic instabilities in many complex fluids, including wormlike micelles,[1–4] liquid crystals,[5–11] and lamellar surfactant systems which can "roll" into multilamellar vesicles ("onions").[12–15] These instabilities typically manifest themselves in non-monotonic constitutive curves such as those in Fig. 1,[16–21] and in several systems, including wormlike micelles and lamellar surfactant solutions, are accompanied by observable coexistence of two macroscopic "phases" of material.

If a mean strain rate forces the system to lie on an unstable part of the flow curve (with negative slope), the system can phase separate into regions (bands) with high and low strain rates and still maintain the applied strain rate.[1,7,18,22] Fig. 1 shows that phase separation can occur at either common stress or common strain rate, depending on the geometry of the bands:[23] bands stacked along the axis of a Couette cell have the same strain rate and different shear stresses, while radial phase separation imposes a uniform shear stress and different strain rates. The shear-thinning wormlike micelle system phase separates radially into common-stress bands, while shear-thickening systems have been observed to separate into bands with both the common stress (worms)[24,25] or common strain rate (worms and onions)[26,27] geometries, although the evidence for true steady state phase separation at common strain rate is not yet firm.

Other systems with flow-induced "phase transitions" include colloidal suspensions of plate-like particles (which shear thicken and sometimes crystallize)[28] or nearly monodisperse spheres,[29] as
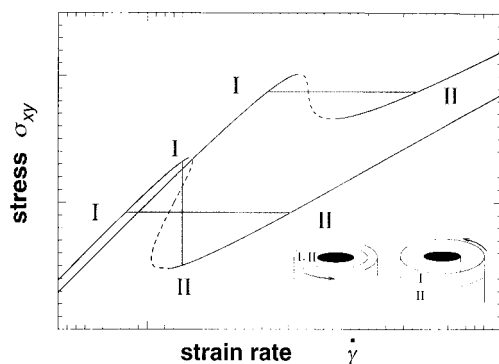
Fig. 1 Stress–strain-rate curves for the Doi model (from Fig. 2) for two concentrations. The dashed lines are unstable steady states. Straight lines indicate possible coexistence (at the same concentration) with either common stress (horizontal lines) or strain rate (vertical line) in the two phases. Inset: geometries for common stress (left) or common strain rate (right) coexistence.

well as a variety of surfactant-like solutions of diblock copolymers in selective solvents.[30] With so many increasingly detailed and careful experiments on so many systems, it would be nice to have a consistent framework for non-equilibrium transitions. Unfortunately, most systems are sufficiently complicated that none of the observed transitions can be completely described, even qualitatively, by a credible microscopic model. For example, in certain limits the class of shear-thinning wormlike micelle systems which shear band has a mature theory for the linear rheology, which may be extended using successful ideas from entangled polymer dynamics to predict an instability.[18] Unfortunately, a complete description of phase coexistence also requires knowledge of the shear-induced state, as well as details of the concentration dependence and, as we shall see, the inhomogeneous contribution to the dynamical equations. We are, at present, far from having all of these ingredients, and in many cases we do not have a clear understanding of even the structure of the high shear rate state, much less its dynamics.

Recently, we have studied a well-known model, the Doi model for rigid rod suspensions in shear flow,[31] which, while admittedly the product of many approximations, provides physically well-founded dynamics for both quiescent and shear-induced states. Although the shear rates necessary for inducing a transition are, in practice, typically quite high unless very long rods are used, and physical systems are often susceptible to various dynamical instabilities, this model system is quite helpful for building intuition about how to calculate non-equilibrium "phase diagrams" and how their resulting topologies resemble and differ from their equilibrium counterparts.

A vexing question for non-equilibrium calculations is how to replace the free energy minimization familiar from equilibrium thermodynamics, to determine the analog of a first order phase transition. In the context of Fig. 1, one needs to determine the selected stress for an imposed strain rate (for phase separation at a common stress). It has emerged that an unambiguous resolution of this problem is to include explicit non-local terms in the dynamical equations and explicitly construct the coexisting state.[7,10,32–34] This reduces to the equilibrium construction in the case of zero shear, and can be shown to yield a single (barring accidental degeneracies) stress (given all other imposed conditions) at which coexistence occurs.[35]

Below we summarize some results of our calculations on the Doi model for rigid rod suspensions in shear flow;[10] the details will be published elsewhere.[36] This system is surprisingly rich, given its apparent simplicity and fairly obvious coupling of internal order to flow. Then we discuss some aspects of the interface construction for determining coexistence, and how it compares to its equilibrium counterpart.

2 The Doi model

The modified Doi model[10,31] describes the dynamics of the rod-like particle suspension. The orientational degrees of freedom are parametrized by the conventional liquid crystalline order

parameter tensor

$$Q_{\alpha\beta}(\mathbf{r}) = \langle v_\alpha v_\beta - \tfrac{1}{3}\delta_{\alpha\beta}\rangle \qquad (1)$$

where $\langle \cdot \rangle$ denotes an average around the point $\mathbf{r}$ of the second moment of the rod orientations $\mathbf{v}$. For rigid rods the phase diagram, and in fact the dynamics, can be more conveniently represented by the excluded volume parameter u, defined by

$$u = \phi L \alpha \qquad (2)$$

where ϕ is the rod volume fraction, L is the rod aspect ratio and α is an $\mathcal{O}(1)$ prefactor.[31] Beginning from the Smoluchowski equation for a solution of rigid rods, and including a Maier–Sauper-like orientational interaction parameter, Doi was able to derive approximate coupled equations of motion for the dynamics of $\mathbf{Q}$ and the fluid velocity $\mathbf{v}(\mathbf{r})$, including the liquid crystalline contribution to the fluid stress tensor.

The essential physics is that flow tends to align the rodlike molecules, typically roughly parallel to the flow direction, and hence stabilizes a nematic, or aligned, state. To study other complex fluids we would have a structural variable analogous to $\mathbf{Q}$; e.g., in the wormlike micelle system we might need, in addition to the orientation tensor, the dynamics of the mean micellar size. We have augmented the Doi model by allowing for concentration diffusion driven by chemical potential gradients, included the dynamical response to inhomogeneities in liquid crystalline order and concentration, and included the translational entropy of mixing, which gives the system a biphasic coexistence regime in the absence of flow. For a given stress or strain rate we determine phase coexistence by explicitly constructing a stable coexisting steady state, which requires inhomogeneous terms in the equations of motion (arising here from free energy terms which penalize inhomogeneities in $\mathbf{Q}$ and ϕ). This procedure and the model have been documented elsewhere,[7,10] and the interface construction will be discussed in more detail in Section 3.

To calculate the phase diagram we solve for the steady state homogeneous solutions to the coupled dynamical equations for $\{\phi, \mathbf{Q}, V\}$. This yields a set of solutions which are then candidates for phase coexistence. Coexistence is possible with either common stress or common strain rate in the coexisting phases, depending on geometry, and must be examined for all pairs of stable homogeneous states. We expect coexisting states to have different values for ϕ, $\mathbf{Q}$, and either the stress or strain rate. As mentioned above, we determine coexistence by finding the locus of control parameters for which a stable interfacial solution between two homogeneous states exists. We parametrize the shear stress and strain rate as

$$\hat{\dot{\gamma}} = \frac{\dot{\gamma} L^2}{6 D_{\mathrm{ro}} v_1 v_2^2} \qquad (3)$$

$$\hat{\sigma}^{xy} = \frac{\sigma_{xy} v_2 L^3}{3 k_{\mathrm{B}} T} \qquad (4)$$

where D_{ro} is the rotational diffusion coefficient, and v_1 and v_2 are $\mathcal{O}(1)$ geometric constants.

The Doi model has three stable steady states in shear flow:[37] A weakly-ordered *paranematic* state I, which the major axis of the order parameter in the shear plane; a *flow-aligning* state N, with a larger order parameter and major axis in the shear plane; and a *log-rolling* state L, with major axis in the vorticity direction. Fig. 2 shows homogeneous constitutive relations for the I and N states. The N and L states are successively less viscous than the I phase at the same concentration, with a viscosity which decreases slightly with increasing concentration (reflecting the greater order and hence lower viscosity of more concentrated phases), in contrast to the less-ordered I phases, whose viscosity increases with concentration, as is usual for colloidal suspensions.

2.1 Common stress phase separation

We first discuss the phase diagrams for common stress coexistence, in which the phase separation is radial in a cylindrical Couette flow. For common stress coexistence of two phases I and II, the
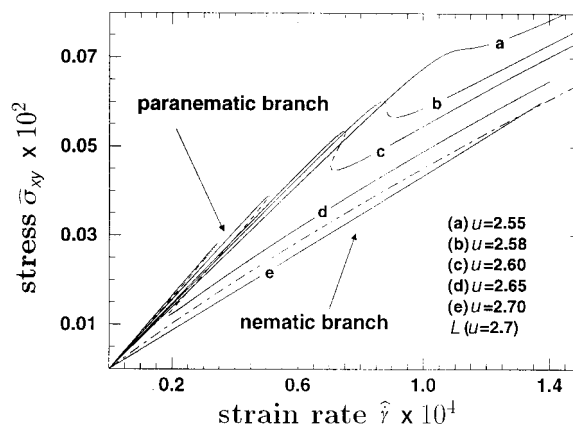
Fig. 2 Homogeneous stress $\hat{\sigma}_{xy}$ vs. strain rate $\hat{\dot{\gamma}}$ curves for various excluded volumes u (u is proportional to ϕ) and $L = 5$. Shown are the I and N branches. The L branch is only stabilized for the high concentration ($u = 2.7$).

fraction ζ in phase I is determined by the lever rule,

$$\bar{\phi} = \zeta\phi_I + (1 - \zeta)\phi_{II} \tag{5a}$$

$$\bar{\dot{\gamma}} = \zeta\dot{\gamma}_I + (1 - \zeta)\dot{\gamma}_{II} \tag{5b}$$

where $\bar{\phi}$ and $\bar{\dot{\gamma}}$ are mean values. Fig. 3 shows the phase diagram calculated for I–N coexistence for $L = 5$. The tie lines denoting pairs of coexisting phases are horizontal in the σ_{xy}–u plane, and have positive slopes in the $\hat{\dot{\gamma}}$–u plane because the more concentrated nematic phase flows faster at a given stress. For weak stresses the equilibrium system is slightly perturbed and the tie lines are almost horizontal, while at high stresses the tie lines become steeper as the composition difference between the phases decreases and vanishes at a critical point.

Mean constitutive relations. From the information in Fig. 3b we can calculate the mean constitutive relation that would be measured in an experiment on a system with a given prescribed mean concentration. Upon applying stress at a given concentration, the system traces a vertical path through Fig. 3 until the two-phase region is reached, during which $\hat{\sigma}_{xy}(\bar{\dot{\gamma}})$ varies smoothly. At this stress a tiny band of N phase develops with composition and strain rate determined by the lever rule; and $\hat{\sigma}_{xy}(\bar{\dot{\gamma}})$ is non-analytic (Fig. 4), exhibiting a change in slope. As the stress and, hence, the
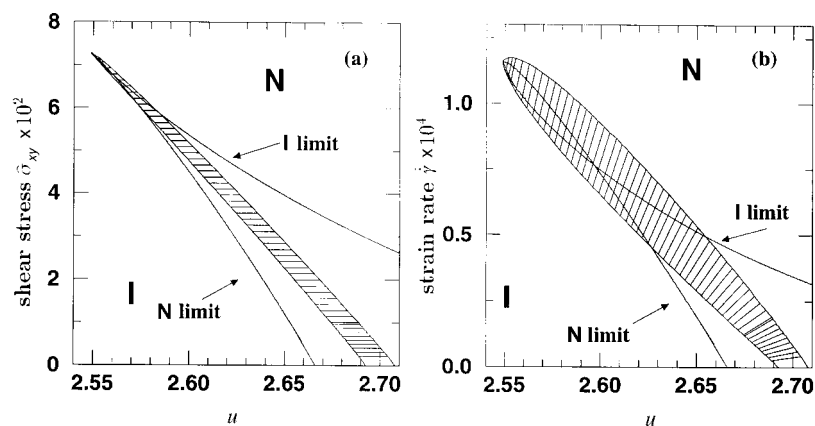
Fig. 3 Phase diagram in the $\hat{\sigma}_{xy}$–u (a) and $\hat{\dot{\gamma}}$–u (b) planes, along with limits of stability of I and N phases. Tie lines [horizontal in (a), sloped in (b)] connect coexisting phases.
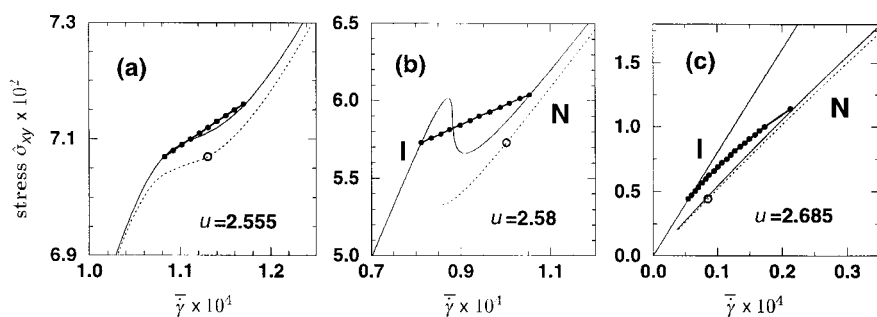
Fig. 4 Stress σ_{xy} *vs.* mean strain rate $\bar{\gamma}$ for common stress coexistence. Solid lines are constitutive curves for the I and N branches; dotted lines and $\bigcirc$ denote the N branch with which each I branch coexists at the low strain rate coexistence boundary. $\bullet$ Denotes banded stresses, whose plateaus do *not* satisfy an equal area construction with the homogeneous constitutive curve.

mean strain rate, increase further the system visits successive tie lines in the $\bar{\gamma}$–u plane, each with a higher stress and mean strain rate and different coexisting concentrations. For $\bar{\phi}$ close to the equilibrium I–N transition (Fig. 4c) the tie lines in the $\hat{\gamma}$–u plane are fairly flat and the stress σ_{xy} changes significantly through the two-phase region. More dilute systems (Fig. 4a and b) have steeper tie lines and straighter and flatter 'plateaus' in $\hat{\sigma}_{xy}(\bar{\gamma})$.

Controlled strain rate experiments should follow the homogeneous flow curves, except for the coexistence regime. In this case, analogy with equilibrium systems suggests that the system should eventually nucleate into a phase-separated banded state, with a corresponding stress change. Experiments on wormlike micelles display this kind of behavior upon increasing the strain rate above that of the phase boundary. If the mean strain rate is on an unstable part of the flow curve, we expect a 'spinodal' (or mechanical) instability. There is a small region (inside the loop in Fig. 3a) where the system is unstable when brought, at controlled strain rate, into this region from either the I or N states. This corresponds to constitutive curves with the shape of curve b in Fig. 2.

For controlled stress experiments, for stresses larger than the minimum coexistence stress and less than the local maximum we expect the system to follow the homogeneous flow curve until a nucleation event occurs (Fig. 4b). Then, the strain rate should increase to either that of proper banded or single N phase strain rate, depending on the magnitude of the stress. For stresses larger than the I limit of stability we expect, again by analogy with equilibrium, a spinodal-type instability. This simple picture is not quite corroborated in wormlike micelles: Grand *et al.* reported that a stress within a narrow range above the coexistence stress could be applied, and the system remained on the "metastable" branch indefinitely.[38]

Analogy with equilibrium systems suggests similar behavior upon reducing the stress or strain rate from the high-shear branch. Careful experiments are needed to test the idea. For example, it is interesting to examine whether upon reducing the strain rate below the upper strain rate for the onset of shear banding and above the limit of stability of the high strain rate branch, the stress would spontaneously increase into the banded state.

Log-rolling phase. Fig. 5 shows the phase diagram for paranematic-log rolling I–L coexistence. For non-zero stress the biphasic region shifts to higher concentrations, since the stability limit of the L phase shifts to higher concentrations. Since the I and L phases have major axes of alignment in orthogonal directions, there is not a critical point; rather, the biphasic region ends when the I phase becomes unstable to the N phase. We have also computed N–L phase coexistence, but cannot resolve this (very concentrated, $u \simeq 3$) regime accurately and do not present these results here.

Can one observe I–L coexistence? This can only occur for concentrations above that necessary for equilibrium phase separation. One could conceivably prepare an equilibrium I–N mixture with the nematic phase in the log-rolling geometry. Upon applying shear, the system would then maintain coexistence and move through the I–L two-phase region. However, the I phase is, itself, within the two-phase region for I–N phase separation, so we expect the prepared coexisting I–L state to be metastable under shear.
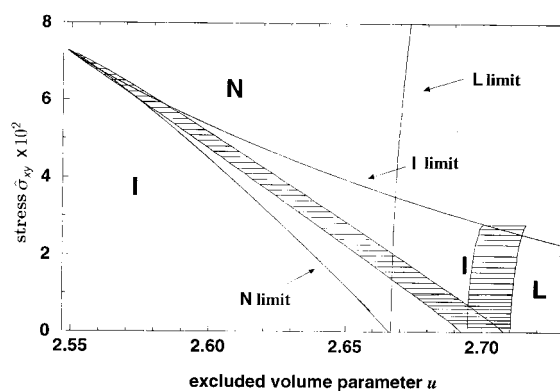
Fig. 5 Composite phase diagrams for I–L and I–N coexistence at common stress. This represents *two* over-layed phase diagrams, and not a single phase diagram.

2.2 Common strain rate phase separation

Common strain rate phase separation can be calculated exactly analogously common stress phase separation. The resulting phase diagram for I–N coexistence, for $L = 5$, is shown in Fig. 6. The shear stress and composition are partitioned according to the lower rule in Fig. 6b, with

$$\bar{\sigma}_{xy} = \zeta\sigma_{xyI} + (1 - \zeta)\sigma_{xyII} \tag{6}$$

In this case tie lines connecting coexisting phases are parallel in the $\dot{\gamma}$–u plane, and have a negative slope in the $\hat{\sigma}_{xy}$–u plane because the I phase coexists with a denser and less viscous N phase. There is an interesting crossover in the $\hat{\sigma}_{xy}$–u plane. For dilute systems the stress in the N phase immediately outside the biphasic regime is *less* than the stress just before the system enters the biphasic region (Fig. 6b). Since the stress of the N branch is less than that of the I branch at the same strain rate and composition, we expect a decrease in the stress across the biphasic regime if composition effects are weak, *e.g.* near a critical point. For higher mean compositions the stress *increases* across the biphasic regime, because the width of the biphasic regime overcomes the shear thinning effect.
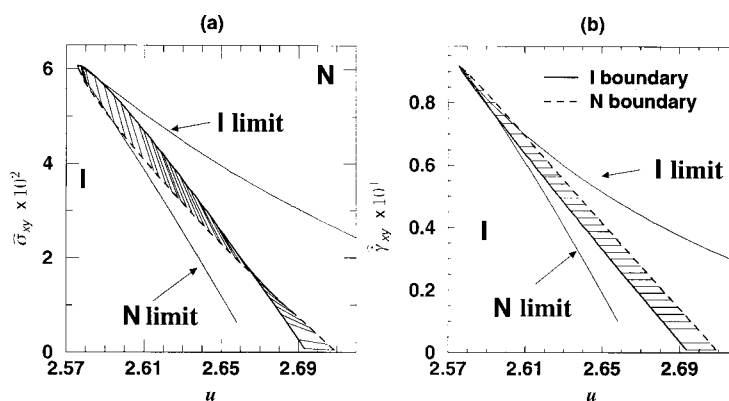
Fig. 6 Common strain rate phase diagram in the $\dot{\gamma}$–u (a) and $\hat{\sigma}_{xy}$–u (b) planes. The solid and dashed lines denote the phase boundaries for, respectively, the I and N phases.

Mean constitutive relations. The mean constitutive relations that could be measured in an experiment may be calculated from Fig. 6a, and are shown in Fig. 7. At higher concentrations the plateau has a positive slope while, coinciding with the crossover noted above, for lower concentrations the plateau has a negative slope. A negative slope usually signifies a bulk instability, but here each band lies on a stable branch of its particular constitutive curve and the flow should be stable. Stable 'negative-slope' behavior has been seen in shear-thickening systems which phase separate at common stress,[24,25] although in that case the mean constitutive curve was different, consisting of a backwards S curve and non-monotonic behavior only with multiple stresses for a given strain rate.

Based on analogies with equilibrium, we naively expect controlled strain rate and controlled stress experiments on concentrations such as those in Fig. 7a and b to yield behavior similar to that for common stress phase separation, with nucleated or spinodal behavior depending on the applied strain rate, and the same caveat applying to decreasing the strain rate from above. The situation for compositions with curves such as Fig. 7a is qualitatively different. Here there is a range of stresses with *three* stable states: homogeneous I and N branches, and a banded intermediate branch. For controlled stress experiments, one possibility is that the I and N branches are favored in their respective domains of stresses. For example, in start-up experiments the system would remain on the I branch until a certain stress, at which point it would nucleate after some time. If the system nucleated onto the coexistence branch, increasing the stress further would return the system to the I branch. Since it nucleated *from* the I branch, it is more likely to jump directly to the N branch. Similar behavior is to be expected upon reducing the stress from the N phase. Another possibility is intrinsic hysteresis: that is, the system never jumps until reaching its limit of stability (from either the I or N side). The present theory cannot address this question. For controlled strain rate experiments, it could, in principle, be possible to maintain a stress on the two-state region, although in practice this would also seem to be quite difficult, and would seem to be mechanically unstable. In the case where stable composite curves with negative slopes were accessed, stress was the control variable.[39]

2.3 Common stress or common strain rate?

What about the relative stability of phase separation at common stress or strain rate? While our one-dimensional calculations cannot address this question, we have examined the two phase diagrams in the σ_{xy}–μ and $\dot{\gamma}$–u planes, where μ is the chemical potential.[10] This can be seen in Fig. 8a and b where, for example, the I boundary for common strain rate phase separation (I_{γ}) lies in the N region for common stress phase separation, in the μ–σ_{xy} plane. This occurs because the stress of the I phase, at common strain rate, is larger than the stress of the N phase, due to the shear thinning nature of the transition. Conversely, the I phase at common stress lies within the I region of the common strain rate phase diagram. Analogy with equilibrium phase transitions suggests that, since the I phase of common strain rate phase separation thus lies on the "wrong" side of the phase boundary for common stress, given by the line in the μ–σ_{xy} plane, it would be unstable (or metastable) to phase separation at common stress. Conversely, the I phase at common stress is on the "correct" side of the coexistence line in the μ–$\dot{\gamma}$ plane, and, again based on analogy with
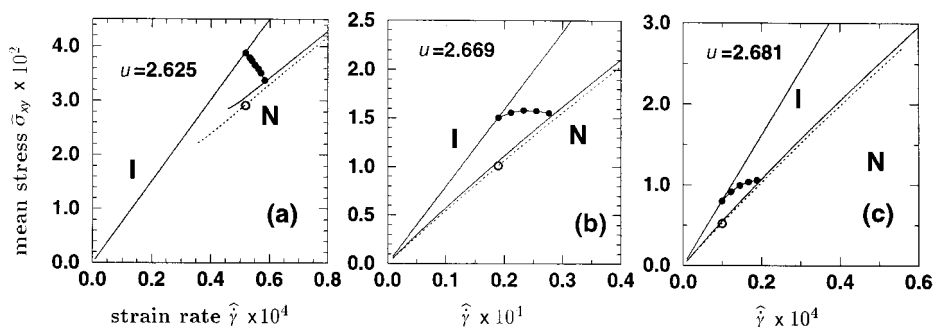
Fig. 7 Stress–strain-rate $\bar{\sigma}_{xy}(\dot{\gamma})$ curves for common strain rate coexistence. Same notation as Fig. 4.

equilibrium, might be expected to be stable. Note that if the transition were shear thickening the situation would be reversed, and the arguments above would lead to common stress phase separation being unstable (or metastable) with respect to common strain rate phase separation.

Boundary conditions may also play a role. In a Couette device the slight inhomogeneity of Couette flow induces an asymmetry between the inner and outer cylinders, exactly the symmetry of common stress phase separation (Fig. 1). This should enhance the stability of common stress phase separation. Cone-and-plate rheometry induces a similar preference for the common stress geometry.

An alternative possibility is presented in Fig. 8, assuming that, in steady state, among the possible phases which are compatible with the interface solvability condition, the chemical potential reaches its minima so that no more diffusive material flux is possible. Based on such a criterion, upon increasing the strain rate for a given mean concentration the stable phase is that with the lowest chemical potential. The thick horizontal arrows in Fig. 8 denote the $\mu(\sigma_{xy})$ and $\mu(\dot{\gamma})$ paths for the homogeneous high and low shear rate states, in the two phase diagrams. The I branch becomes unstable at A to phase separation at common stress, when the homogeneous path first crosses the phase boundary in the μ–σ plane. For higher stresses the system follows the segment AB in Fig. 8b, along the phase coexistence line at common stress, and follows the stress plateau AB in Fig. 8c. In the μ–$\dot{\gamma}$ plane the system phase separates, and the chemical potential as a function of mean strain rate follows the diagonal path AB in Fig. 8a (the dotted lines denote the strain rates of the coexisting phases).

Upon increasing the strain rate further than point B, the chemical potential of the system can decrease by phase separating at a common strain rate. This reduces the chemical potential, at a given strain rate, from that of the segment BD to that of segment BC. Hence the system would take the path BC along the phase boundary in the μ–$\dot{\gamma}$ plane, as far as point C, upon which the phase boundary crosses the homogeneous curve for the high strain rate phase of the given mean concentration. The path would be the diagonal path BC in the μ–σ_{xy} plane, and would correspond to the negative-sloped segment BC in the flow curve, Fig. 8c. Finally the system follows the high strain rate branch, through CD.

Upon increasing the controlled stress, the system would be expected to follow ABD. Upon decreasing the stress or the strain rate, DC-bottom jumping is expected. These scenarios follow from minimizing the chemical potential subject to the solvability constraint should phases coexist.
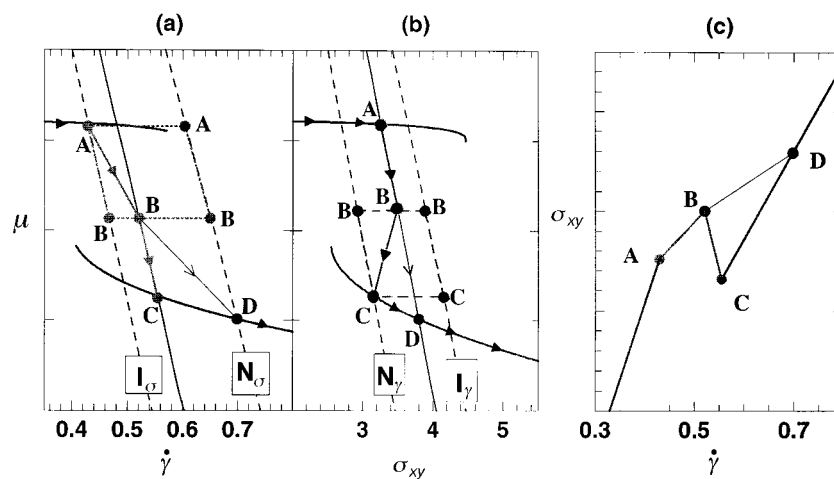
Fig. 8 Phase diagrams in the (a) μ–$\dot{\gamma}$ and (b) μ–σ_{xy} planes for I–N coexistence (the N state is stable for higher strain rate or stress, respectively). The thin vertical solid lines denote phase coexistence at common strain rate and stress in (a) and (b), respectively. The broken lines marked I_{γ} and N_{γ} denote the coexisting states at common strain rate, in the μ–σ_{xy} plane (b); while the broken lines I_{σ} and N_{σ}, denote the coexisting states at common stress, in the μ–$\dot{\gamma}$ plane. (c) Is the mean stress $vs.$ strain rate curve. ABD denotes a path in the phase diagrams for common stress phase separation, while ABCD is a path which switches from common stress phase separation to common strain rate phase separation B.

Its correctness, of course, should be further examined by the full time evolution of the original dynamic equations.

Experimental studies. Mather *et al.*[8] studied a liquid crystalline polymer melt (an aromatic polyester) and determined the lower limit of the l–N phase boundary in the $\dot{\gamma}$–T plane. The studies most relevant to the Doi model for rigid rod suspensions have been on wormlike micellar solutions near the isotropic–nematic coexistence region,[1,40] where common-stress banding was observed with a plateau stress that became steeper for concentrations closer to the equilibrium l–N phase boundary, in qualitative agreement with our results. Common strain rate banding has not been seen in these systems. Micelles are considerably more complicated than simple rigid rods, because they are not strictly rigid and their length (and hence coupling to flow) is a strong dynamic function of concentration. Experiments on micelles far from an apparent nematic transition exhibit common stress shear banding with nearly flat coexistence plateaus,[1,20,22,38,41] consistent with a concentration-independent[19] instability (or transition). In kinetics studies the delay time before the transition to a banded (or high strain rate) flow in controlled stress start-up 'quenches' diverged for a window of stresses slightly above the banding stress, whereas controlled strain rate 'quenches' always decayed, eventually, onto a banded flow state. These interesting behaviors cannot be explained by the topologies of the phase diagrams in Fig. 3. Bonn *et al.*[27] recently studied lamellar surfactant systems and observed slowly coarsening bands in the common strain rate geometry; and for controlled strain rate measurements they found transient constitutive curves analogous to Fig. 7a or b, consistent with common strain rate phase separation. The true study state behavior was not measured.

3 Interface construction

Several microscopic and phenomenological models, as well as the apparent underlying flow curves for wormlike micelles, show an apparent degeneracy in the shear stress at which coexistence occurs (in the case of coexistence at a common stress). To resolve this degeneracy we have relied on the presence of inhomogeneous terms in the dynamical equations of motion, and determined the selected stress as that stress which allows a stable interfacial solution. In this section we explore this in more detail using a toy constitutive model. Similar arguments were given by Spenley *et al.*[33] in a different language, and in a recent more rigorous study.[35]

We consider planar flow with a velocity field $\boldsymbol{v}(r) = v(y)\hat{\boldsymbol{x}}$, with $\dot{\gamma}(y) \equiv \partial v/\partial y$, and postulate the following constitutive relation for the shear stress:

$$\sigma(\dot{\gamma}) = \sigma_{\mathrm{h}}(\dot{\gamma}) - D(\dot{\gamma})\partial_y^2 \dot{\gamma} \tag{7}$$

The homogeneous flow curve $\sigma_{\mathrm{h}}(\dot{\gamma})$ is non-monotonic, as in Fig. 9, and can be derived for a system with an underlying transition, such as the modified Doi model above, or from phenomenological models, such as the widely-used Johnson–Segalman (JS) model.[42] Gradient terms may come from the diffusion of the stress elements.[43] The flow curve shown in Fig. 9 is for the JS model. In the
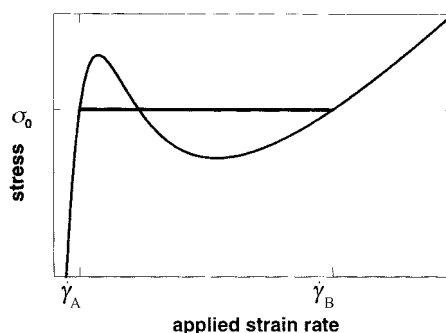
Fig. 9 Non-monotonic homogeneous flow curve $\sigma_{\mathrm{h}}(\dot{\gamma})$ for the Johnson–Segalmann model. The thick curve denotes a banded flow between strain rates $\dot{\gamma}_{\mathrm{A}}$ and $\dot{\gamma}_{\mathrm{B}}$ at stress σ_0.

(some what artificial) model where only the shear stress diffusion is considered, the steady flow condition for the JS model has the form of eqn. (7), with $D(\dot{\gamma}) \propto 1/(1 + \dot{\gamma}^2)$.

The steady state condition for planar flow is a uniform shear stress,

$$\sigma_0 = \sigma_h(\dot{\gamma}) - D(\dot{\gamma})\partial_y^2 \dot{\gamma} \qquad (8)$$

with σ_0 a constant. In an infinite system, an interfacial shear banding solution at a given stress σ_0 satisfies eqn. (8), with boundary conditions

$$\dot{\gamma}(-\infty) = \dot{\gamma}_A \qquad (9a)$$

$$\dot{\gamma}(\infty) = \dot{\gamma}_B \qquad (9b)$$

$$\partial_y \dot{\gamma}(\pm\infty) = 0 \qquad (10)$$

Hence, given the second-order differential equation, the system is overdetermined. A solution is only possible when these two conditions coincide, which may be obtained by varying the stress σ_0. It is straightforward to integrate eqn. (8) to show that a solution is possible when σ_0 satisfies the following condition[35]

$$\int_{\dot{\gamma}_A}^{\dot{\gamma}_A} \frac{\sigma_0 - \sigma_h(\dot{\gamma})}{D(\dot{\gamma})} = 0 \qquad (11)$$

Note that this is not an equal areas construction, unless $D(\dot{\gamma})$ is a constant D.

Further insight may be obtained by casting the interface solution in terms of a dynamical system. Defining

$$p = \dot{\gamma} \qquad (12a)$$

$$q = \partial_y p \equiv p' \qquad (12b)$$

Eqn. (8) becomes the following dynamical system, with y playing the role of time.

$$p' = q \qquad (13a)$$

$$q' = \frac{\sigma_0 - \sigma_h(p)}{D(p)} \qquad (13b)$$

For σ_0 within the non-monotonic region of the flow curve the system has three fixed points $p_* = \{p_A, p_B, p_C\}$ on the axis $q = 0$, corresponding to the strain rates of the three homogeneous flows. Linear stability analysis yields the stable and unstable manifolds of point A and B, with eigenvalues

$$\lambda_{\pm} = \pm \sqrt{\left[\frac{1}{D(p)} \frac{d\sigma_h}{dp}\right]\bigg|_{p=p_*}} \qquad (14)$$

and eigenvectors at angles $\theta = \arctan \lambda$ with respect to the p-axis. Point C has imaginary eigenvalues and is a cycle, while A and B are saddles with stable and unstable directions.

An interfacial solution corresponds to an orbit connecting saddles A and B, and is denoted a saddle connection; it is also called a heteroclinic orbit, since it connects two different fixed points. This set of ordinary differential equations (ODE) does not generally have a saddle connection for an arbitrary σ_0 in the multi-valued region. It can be shown[35] for models (with arbitrary numbers of dynamical variables) in planar shear flow with differential non-local terms that, apart from accidents, a saddle connection only exists at isolated points in the control parameter space. Here, the control parameters are σ_0 and parameters which change the shape of σ_h,[33,35] while for the Doi model above, the control parameters are (for a given set of molecular parameters such as L) μ and σ_{xy} for common stress phase separation, and μ and $\dot{\gamma}$ for common strain rate phase separation.

Fig. 10 shows the evolution of "orbits" in the p–q phase space as the stress is tuned. For $\sigma = \sigma_0$ a heteroclinic orbit exists, connecting A and B. This corresponds to an elementary shear band solution, in which one portion of the sample lies on the high strain rate branch B, another portion lies on the low strain rate branch A, and a single interface separates the two phases. For $\sigma \neq \sigma_0$
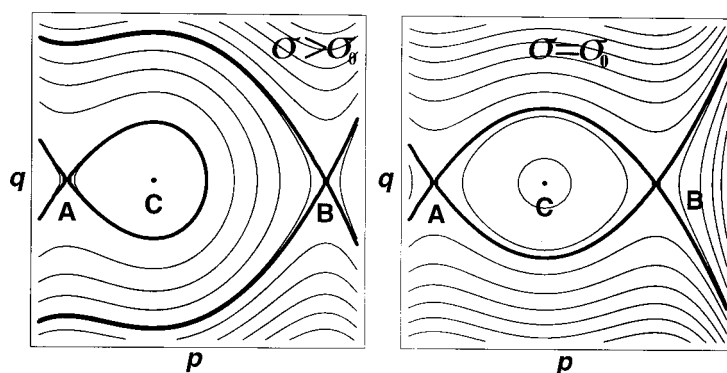
Fig. 10 Orbits in the phase space for the dynamical system of eqn. (13). (Left) Away from the coexistence stress, $\sigma > \sigma_0$, a saddle connection does not exist and A is connected to itself by a homoclinic orbit. [A similar situation exists for $\sigma < \sigma_0$, with the homoclinic orbit returning to B instead of A.] (Right) At the coexistence stress $\sigma = \sigma_0$ a heteroclinic orbit connecting A and B (saddle connection) exists. The fixed points are at $q = 0$, and the solid lines show orbits beginning and ending on the stable fixed points A and B.

there is no heteroclinic orbit or saddle connection, and hence no stationary interface. Fig. 10 (left) shows a stress slightly greater than σ_0, with a homoclinic orbit connecting state A to itself. Kramer[32] pointed out in the context of reaction diffusion equations that such a homoclinic orbit corresponds to the critical droplet in a metastable phase of A material. Note that, although in real space it extends from A at $y = -\infty$ to A at $y = +\infty$, the dominant spatial variation is in fact localized, with a size that vanishes when the stress reaches the maximum of the flow curve in Fig. 9 (at which the fixed points A and C annihilate). Slightly larger droplets are unstable and, when the full dynamics are returned to the problem, presumably flow to the high strain rate branch B, while smaller droplets are expected to decay back to A. By analogy with equilibrium behavior, for $\sigma > \sigma_0$ we expect phase B to be the long time steady state, if fluctuations (*i.e.* noise, thermal or otherwise) were included.

4 Conclusion

We have outlined the phenomenology of phase separation of rigid rod suspensions in shear flow, using the modified Doi model. Phase separation may occur with common stress *or* strain rate, corresponding to the different coexistence geometry. We have calculated coexistence among three phases (paranematic, flow-aligning nematic, and log-rolling), while only two equilibrium phases exist. That is, the full rotational symmetry of an equilibrium nematic is broken by the biaxial shear flow, leaving two possible stable nematic orientations (the in-plane I and N states, and the out of plane L state). The shear thinning nature of the transition suggests that common stress phase separation is stable; while appealing to a minimization of the chemical potential, subjected to the interface solvability, predicts a curious crossover from common stress to common strain rate phase separation. We do not know which of these, or other, possibilities, are the physical ones. The composite stress strain curves depend on the coupling to composition,[23] and can exhibit an apparent unstable constitutive relation, which would be mechanically unstable under controlled strain rate conditions. Although there have been few experiments on true lyotropic rigid rod systems in flow, wormlike micelles can have a flow-induced nematic phase at higher concentrations, and our results appear to qualitatively describe many aspects of these experiments. See, for example, the phase diagrams in ref. 44.

We have also shown schematically how our construction for coexistence can be cast as an equivalent dynamical system, for which coexistence corresponds to a heteroclinic saddle connection. In the most general case, stress selection depends on the nature of the gradient terms in the dynamics,[35] while in equilibrium systems the gradient terms can be exactly integrated to yield a condition independent of the gradient terms. The dynamical systems picture also yields an

analogy with a critical droplet, which may prove promising in understanding the non-equilibrium analogs of nucleation and growth.

Acknowledgements

References

1 J. F. Berret, D. C. Roux, G. Porte and P. Lindner, *Europhys. Lett.*, 1994, **25**, 521.
2 J. F. Berret, D. C. Roux and G. Porte, *J. Phys. II*, 1994, **4**, 1261.
3 J. F. Berret, G. Porte and J. P. Decruppe, *Phys. Rev. E: Stat. Phys., Plasmas, Fluids, Relat. Interdiscip. Top.*, 1997, **55**, 1668.
4 E. Cappelaere, J. F. Berret, J. P. Decruppe, R. Cressely and P. Lindner, *Phys. Rev. E: Stat. Phys., Plasmas, Fluids, Relat. Interdiscip. Top.*, 1997, **56**, 1869.
5 S. Hess, *Z. Naturforsch. A: Phys. Sci.*, 1976, **31**, 1507.
6 P. D. Olmsted and P. M. Goldbart, *Phys. Rev. A*, 1990, **41**, 4578.
7 P. D. Olmsted and P. M. Goldbart, *Phys. Rev. A.*, 1992, **46**, 4966.
8 P. T. Mather, A. Romo-Uribe, C. D. Han and S. S. Kim, *Macromolecules*, 1997, **30**, 7977.
9 H. See, M. Doi and R. Larson, *J. Chem. Phys.*, 1990, **92**, 792.
10 P. D. Olmsted and C-Y. D. Lu, *Phys. Rev. E: Stat. Phys., Plasmas, Fluids, Relat. Interdiscip. Top.*, 1997, **56**, 55.
11 C. R. Safinya, E. B. Sirota and R. J. Plano, *Phys. Rev. Lett.*, 1991, **66**, 1986.
12 M. E. Cates and S. T. Milner, *Phys. Rev. Lett.*, 1989, **62**, 1856.
13 D. Roux, F. Nallet and O. Diat, *Europhys. Lett.*, 1993, **24**, 53.
14 O. Diat, D. Roux and F. Nallet, *J. Phys. II*, 1993, **3**, 1427.
15 O. Diat, D. Roux and F. Nallet, *Phys. Rev. E: Stat. Phys., Plasmas, Fluids, Relat. Interdiscip. Top.*, 1995, **51**, 3296.
16 M. Doi and S. F. Edwards, *The Theory of Polymer Dynamics*, Clarendon, Oxford, 1989.
17 M. E. Cates, T. C. B. McLeish and G. Marrucci, *Europhys. Lett.*, 1993, **21**, 451.
18 N. A. Spenley, M. E. Cates and T. C. B. McLeish, *Phys. Rev. Lett.*, 1993, **71**, 939.
19 M. E. Cates, *J. Phys. Chem.*, 1990, **94**, 371.
20 H. Rehage and H. Hoffmann, *Mol. Phys.*, 1991, **74**, 933.
21 T. C. B. McLeish and R. C. Ball, *J. Polym. Sci. Part B: Polym. Phys.*, 1986, **24**, 1735.
22 M. M. Britton and P. T. Callaghan, *Phys. Rev. Lett.*, 1997, **78**, 4930.
23 V. Schmitt, C. M. Marques and F. Lequeux, *Phys. Rev. E: Stat. Phys., Plasmas, Fluids, Relat. Interdiscip. Top.*, 1995, **52**, 4009.
24 P. Boltenhagen, Y. T. Hu, E. F. Matthys and D. J. Pine, *Europhys. Lett.*, 1997, **38**, 389.
25 P. Boltenhagen, Y. T. Hu, E. F. Matthys and D. J. Pine, *Phys. Rev. Lett.*, 1997, **79**, 2359.
26 E. K. Wheeler, P. Fischer and G. G. Fuller, *J. Non-Newtonian Fluid Mech.*, 1998, **75**, 193.
27 D. Bonn, J. Meunier, O. Greffier, A. Alkahwaji and H. Kellay, *Phys. Rev. E: Stat. Phys., Plasmas, Fluids, Relat. Interdiscip. Top.*, 1998, **58**, 2115.
28 A. B. D. Brown, PhD Thesis, Cambridge University, 1998.
29 M. D. Haw, W. C. K. Poon and P. N. Pusey, *Phys. Rev. E: Stat. Phys., Plasmas, Fluids, Relat. Interdiscip. Top.*, 1998, **57**, 6859.
30 O. Diat, G. Porte and J. F. Berret, *Phys. Rev. B*, 1996, **54**, 14 869.
31 M. Doi, *J. Polym. Sci. Polym. Phys. Ed.*, 1981, **19**, 229.
32 L. Kramer, *Z. Phys. B: Condens. Matter*, 1981, **41**, 357.
33 N. A. Spenley, X. F. Yuan and M. E. Cates, *J. Phys. II*, 1996, **6**, 551.
34 J. R. A. Pearson, *J. Rheol. (NY)*, 1994, **38**, 309.
35 C-Y. D. Lu, P. D. Olmsted and R. C. Ball, 1999, *Phys. Rev. Lett.*, submitted.
36 P. D. Olmsted and C-Y. D. Lu, *Phys. Rev. E: Stat. Phys., Plasmas, Fluids, Relat. Interdiscip. Top.*, submitted.
37 A. V. Bhave, R. K. Menon, R. C. Armstrong and R. A. Brown, *J. Rheol. (NY)*, 1993, **37**, 413.
38 C. Grand, J. Arrault and M. E. Cates, *J. Phys. II*, 1997, **7**, 1071.
39 Y. T. Hu, P. Boltenhagen and D. J. Pine, *J. Rheol. (NY)*, 1998, **42**, 1185.
40 V. Schmitt, F. Lequeux, A. Pousse and D. Roux, *Langmuir*, 1994, **10**, 955.
41 J. F. Berret, *Langmuir*, 1997, **13**, 2227.
42 M. Johnson and D. Segalman, *J. Non-Newtonian Fluid Mech.*, 1977, **2**, 255.
43 A. W. El-Kareh and L. G. Leal, *J. Non-Newtonian Fluid Mech.*, 1989, **33**, 257.
44 E. Cappelaere, R. Cressely and J. P. Decruppe, *Colloids Surf. A*, 1995, **104**, 353.